Solar Energy 194 (2019) 656–670

Contents lists available at ScienceDirect

Solar Energy

journal homepage: www.elsevier.com/locate/solener

Coyote optimization algorithm for the parameter extraction of photovoltaic cells

Vun Jack Chin[a,b,c,*], Zainal Salam[b,c,*]

[a] School of Electronics and Computer Science, University of Southampton Malaysia, 79200 Iskandar Puteri, Malaysia
[b] Centre of Electrical Energy Systems, School of Electrical Engineering, Universiti Teknologi Malaysia, Johor Bahru, Malaysia
[c] Institute of Future Energy, Universiti Teknologi Malaysia, Johor Bahru, Malaysia

ARTICLE INFO

Keywords:
Solar photovoltaic
Parameter extraction
Coyote optimization algorithm
Evolutionary algorithm
Equivalent circuit model

ABSTRACT

In this paper, a new and powerful metaheuristic optimization technique known as the Coyote Optimization Algorithm (COA) is proposed for the parameter extraction of the PV cell/module. It is utilized to identify the parameters of the single diode and two-diode models. Inspired by the social norms adopted by the coyotes to ensure the survivability of their species, the COA possesses several outstanding merits such as low number of control parameters, ease of implementation and diverse mechanisms for balancing exploration and exploitation. For physically meaningful solutions, a set of parametric constraints is introduced to prevent the coyotes from straying outside of the predefined boundaries of the search space. Extensive tests indicate that the proposed optimizer exhibits superior accuracy compared to other state-of-the-art EA-based parameter extraction methods. It achieved root-mean-square error (RSME) as low as 7.7301E-04 A and 7.3265E-04 A, for the single-diode and two-diode models, respectively. Moreover, the algorithm maintains outstanding performance when tested on an assortment of modules of different technologies (i.e. mono-crystalline, poly-crystalline, and thin film) at varying irradiance and temperature. The standard deviations (STDs) of the fitness values over 35 runs are measured to be less than 1×10^{-5} for both models. This suggests that the results produced by the algorithm are highly consistent. With these outstanding merits, the COA is envisaged to be a competitive option for the parameter extraction problem of PV cell/module.

1. Introduction

To date, solar PV is among the fastest-growing sources of energy in the world. According to the latest global status report by REN21, the world added at least 98 GW of solar PV capacity in 2017—which surpasses the capacity installed from any other type of power generating technology for the same duration (Secretariat, 2018). Putting that into perspective, the current capacity is equivalent to an average of more than 40,000 solar modules being installed each hour of the year. However, unlike conventional energy sources (such as fossil fuels), the output of a PV system is highly dependent on the availability of solar irradiance (Chin et al., 2015c; Virtuani and Strepparava, 2017). Furthermore, although the commercial modules are normally associated with performance warranty periods of up to 25 years, PV systems are typically deployed under harsh operating conditions—which inevitably leads to accelerated degradation (Rajput et al., 2016a; Rajput et al., 2016b). Therefore, the availability of a tool which accurately characterizes the performance of the PV modules for varying meteorological conditions is indispensable.

More than 90% the PV cells in use today, i.e. monocrystalline, polycrystalline and thin film, are silicon-based ((ISE), 2018). Thus, their characteristics can be conveniently described using the electrical-based diode models (Chin et al., 2016; Oliva et al., 2017a; Yu et al., 2017). In these models, lumped elements (also known as *model parameters*) are used to describe the electrical properties and physical phenomena that transpire within the cells. For instance, the current source represents the photo-generated current; while the series resistor accounts for the losses due to the contact resistance between silicon and electrodes surfaces, and the innate resistance of the materials (Chin et al., 2015b). There are also other emerging cell technologies such as the perovskite (Moeini et al., 2018), organic (De Castro et al., 2016; Jain and Kapoor, 2005; Yu et al., 2018a) and multi-junction (Ben Or and Appelbaum,

* Corresponding authors at: Centre of Electrical Energy Systems, School of Electrical Engineering, Universiti Teknologi Malaysia, 81310 Johor Bahru, Malaysia; Institute of Future Energy, Universiti Teknologi Malaysia, Johor Bahru 81310, Malaysia. Tel.: +60 7 553 6187; fax: +60 7 556 6272 (Z. Salam). University of Southampton Malaysia, School of Electronics and Computer Science, 79200 Iskandar Puteri, Malaysia. Tel.: +60 7 560 2443 (V.J. Chin).
E-mail addresses: c.vun-jack@soton.ac.uk (V.J. Chin), zainals@fke.utm.my (Z. Salam).

https://doi.org/10.1016/j.solener.2019.10.093
Received 17 February 2019; Received in revised form 27 October 2019; Accepted 31 October 2019
Available online 13 November 2019
0038-092X/

2013). However, owing to their distinctive physical structures and materials, the characterization of these cells requires specialized models—which are beyond the scope of this work.

The precise knowledge of model parameters is vital for numerous practical applications. For instance, they are utilized extensively in the industry to simulate and emulate the performance of PV systems prior to installation (Chin et al., 2017; Ram et al., 2018; Zagrouba et al., 2010). The procedure is crucial for accurate energy yield prediction and characterization of the power converter hardware. In (Kahoul et al., 2014; Kichou et al., 2016; Malvoni et al., 2017; Meyer and Dyk, 2004), they are used to assess the reliability and degradation rates of the PV modules. Another field where the parameters are instrumental is in the quality control of the PV cell manufacturing process (Sellami and Bouaïcha, 2011). Nonetheless, due to the presence of exponential terms and transcendental nature of the model equations, the parameter extraction process is computationally challenging (Oliva et al., 2017a). Besides, the output characteristics of the modules differ from one to another depending on the operating conditions, age, materials, and the manufacturing technique employed (Femia et al., 2012; Jamil et al., 2017; Park et al., 2013). For these reasons, the problem has garnered the interest of numerous researchers over the past decades, and various computational methods have been proposed (Chin et al., 2015b).

The available parameter extraction methods can generally be classified into two groups: analytical methods and numerical methods. The former determines the parameters by solving a system of equations that is derived from several key information of the *I-V* characteristics, such as the open circuit voltage, short circuit current, maximum power point and temperature coefficients. Since these specifications are typically provided on the standard module datasheet, the analytical methods are inherently convenient. Despite the advantage, they are more susceptible to measurement noise as only few selected points are taken into consideration (Ishaque et al., 2011). Furthermore, to make the computation analytically manageable, these methods often rely on approximations which lead to inaccurate and physically unrealistic solutions (Chin et al., 2015b; Chin et al., 2017; Ishaque et al., 2012). Also, since the datasheets values refer to newly manufactured modules, the solutions are not applicable to on-site modules that have undergone substantial degradation (Jamil et al., 2017).

On the other hand, the numerical methods compute the parameters by minimizing the difference between the simulated *I-V* curve and the experimental data points. The latter is usually acquired using a monitoring hardware setup or extracted directly from the module datasheet. The numerical approach is recognized to be more reliable than its analytical counterpart (Chin et al., 2017; Lin et al., 2017). The algorithm itself can be categorized into two types: deterministic and heuristic. Deterministic methods are generally gradient-based—examples include the least-square Newton-Raphson method (Easwarakhanthan et al., 1986), Levenberg–Marquardt algorithm (Gow and Manning, 1999; Ikegami et al., 2001), Runge-Kutta method (Elbaset et al., 2014), iterative curve-fitting (Chan and Phang, 1987), and conductivity method (Chegaar et al., 2001). Notwithstanding their efficacies in local search, a common disadvantage among these methods is the requirement for continuity, convexity and differentiability of the objective function. It is also known that the improper choice of initial values could result in non-convergence. Plus, the performance of the optimizer tends to deteriorate as the number of decision parameters increases (El-Naggar et al., 2012; Saha et al., 2015).

To overcome these shortcomings, various heuristic optimization algorithms such as the evolutionary algorithms (EAs) have been applied for the parameter extraction problem; they include the genetic algorithm (GA) (Jervase et al., 2001; Moldovan et al., 2009; Sellami and Bouaïcha, 2011; Zagrouba et al., 2010), particle swarm optimization (PSO) (Hengsi and Kimball, 2011; Jing Jun and Kay-Soon, 2012; Sandrolini et al., 2010; Wei et al., 2011; Ye et al., 2009), differential evolution (DE) (Chin and Salam, 2019; da Costa et al., 2010; Gong and Cai, 2013; Ishaque et al., 2012), simulated annealing (SA) (El-Naggar et al., 2012), cuckoo search (CS) (Ma et al., 2013), harmony search (HS) (Askarzadeh and Rezazadeh, 2012), pattern search (PS) (AlHajri et al., 2012; AlRashidi et al., 2011), artificial bee swarm optimization (ABSO) (Askarzadeh and Rezazadeh, 2013a), the bird mating optimizer (BMO) (Askarzadeh and Rezazadeh, 2013b), artificial bee colony (ABC) (Jamadi et al., 2016; Oliva et al., 2014), and chaotic whale optimizer algorithm (CWOA) (Oliva et al., 2017a). In contrast to the deterministic approach, these methods are known for their effective global search and ability to handle non-linear function without gradient information. Moreover, owing to their stochastic nature, the final solutions of these algorithms are independent of the initial guess. Numerous works have shown that EAs provide more accurate and robust solutions than the deterministic algorithms (AlRashidi et al., 2011; Askarzadeh and Rezazadeh, 2012; Ye et al., 2009). However, the EAs usually contain many algorithm-specific parameters (also known as *control parameters*) which must be carefully adjusted to suit specific problems. The inappropriate settings could result in slow convergence rate and premature convergence (Eiben et al., 1999; Jiang et al., 2013). Further, depending on the nature of the search surface, the EAs could get stuck in local optimums (Askarzadeh and Rezazadeh, 2013a; Gao et al., 2018). In fact, due to the multi-modal nature of the PV parameter extraction problems, most available EAs fail to obtain the global optimal solution. Considering that the exact values of the model parameters are not known, any enhancement in fitting accuracy is considered highly valuable from the modelling point of view. Moreover, according to the No Free Lunch theorem (Wolpert and Macready, 1997), no single algorithm is suitable to solve for all optimization problems. Thus, the search for an alternative optimization algorithm that can reliably identify the PV model parameters is an active field of research.

The effectiveness of an EA depends on its balance between exploration and exploitation (Tan et al., 2009). Exploration denotes the diversification of the algorithm's population to probe new regions of the search space; whereas exploitation refers to the ability to refine the existing solutions by searching around their proximities. Inspired by the social structure of coyotes (or *canis latrans* species), the Coyote Optimization Algorithm (COA) is one of the most recent EAs available in the literature (Coelho, 2018). The new algorithm formulates a unique strategy and diverse mechanisms for balancing exploration and exploitation by mimicking the social organization and adaptation strategies of the coyotes. The algorithm has a very simple structure and comprises only two control parameters, i.e. N_p and N_c. Therefore, it is simple to implement and does not require extensive trial-and-errors for tuning the parameters. Despite its simplistic nature, the COA is proven to substantially outperform other nature-inspired metaheuristics in 92 case studies according to the non-parametric Wilcoxon-Mann-Whitney and Friedman statistical significance tests (Coelho, 2018). Notwithstanding the promising potentials, a comprehensive search of the literature reveals that the COA has yet to be applied for the parameter extraction of solar cell models.

In light of the preceding discussions, this study presents a seminal effort to apply the COA to the field of PV cell modelling. To this end, the COA is applied to extract the model parameters of PV cells and modules for the single diode and the two-diode models. To ensure effective implementation of COA, a simple procedure is utilized to determine the optimal control parameter settings. The root-mean-square error (RMSE) between the PV model output and the experimental data points is defined as the objective function to be minimized. Further, this work introduces a set of parametric constraints to confine the search within the predefined parameters boundaries. For validation, the results are evaluated against other popular algorithms based on two widely

utilized datasets as benchmarks, i.e. the R.T.C France 57 mm diameter silicon solar cell and Photowatt-PWP 201 polycrystalline module. In addition, the algorithm is tested on three PV modules of different technologies (mono-crystalline, multi-crystalline, and thin film) at varying levels of irradiance and temperature. The simulation results reveal that the performance of the COA is highly competitive, i.e. it achieves substantially more accurate solutions than other related state-of-the-art EAs. Besides, the algorithm is observed to be highly consistent and effective for practical applications.

The rest of the paper is arranged as follows: Section 2 describes the concepts behind the single diode and two-diode model; Section 3 formulates the objective functions of the optimization problem. Section 4 briefly elaborates the basics of the COA; Section 5 presents and discusses in detail the results obtained by the proposed algorithm and other related works for three well-established case studies. Moreover, the performance when tested on another three commercial modules at various environmental conditions is also discussed. Finally, a conclusion of the work is given in Section 6.

2. Mathematical models of the solar cell

To accurately describe the output characteristics of the solar cell, it is crucial to employ a mathematical model that adequately describe the physical phenomena that take place in the *p-n* junction. In this regard, the single diode and two-diode model are the most utilized (Chin et al., 2015b). By assuming the PV cells to be identical and operating under uniform conditions, the following section explains the concepts behind the single and two-diode models and how they can be formulated as objective functions for parameter extraction purposes.

2.1. Single diode model

Fig. 1 illustrates the circuit topology of the single diode model of the PV cell. The model comprises a current source connected in parallel to a simple *p-n* diode and a shunt resistance (R_{sh}), and in series with a series resistance (R_s). By Kirchhoff's Current Law (KCL), the output current of the solar cell can be express as follows (Chin and Salam, 2018):

$$I = I_{pv} - I_d - I_{sh} \tag{1}$$

where I denotes the terminal current, I_{pv} is the photo-generated current, I_d is the current through the diode, and I_{sh} is the shunt resistance current. According to Shockley's diode equation, I_d can be written as,

$$I_d = I_o\left(e^{\frac{V+IR_s}{aV_t}} - 1\right) \tag{2}$$

where I_o and a describe the saturation current and ideality factor of the diode, respectively. $V_t\ (=N_skT/q)$ is the thermal voltage for PV cell. k represents the Boltzmann constant ($1.3806503 \times 10^{-23}$ J/K). Meanwhile, q is the electron charge ($1.60217646 \times 10^{-19}$C) and T denotes the cell temperature in kelvin (K).

On the other hand, the expression for I_{sh} can be expounded as,

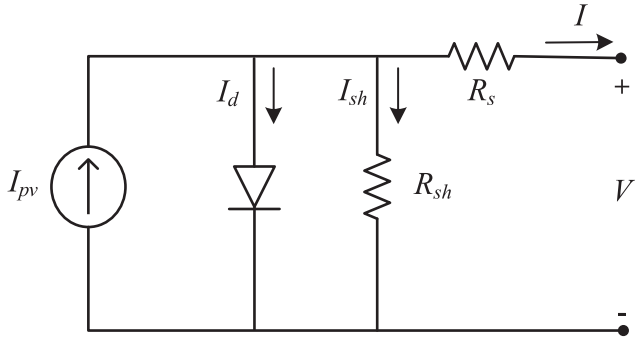

Fig. 1. Circuit topology of the single diode model.

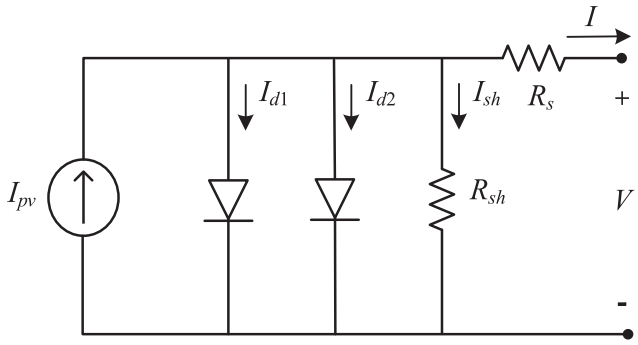

Fig. 2. Circuit topology of the two-diode model.

$$I_{sh} = \frac{V + IR_s}{R_{sh}} \tag{3}$$

By substituting Eqs. (2) and (3) into Eq. (1), and taking into consideration the connection of the cells, the current output of a PV cell/module can be written as,

$$I = I_{pv}N_p - I_oN_p\left(e^{\frac{V+IR_s(N_s/N_p)}{aV_t}} - 1\right) - \frac{V + IR_s(N_s/N_p)}{R_{sh}(N_s/N_p)} \tag{4}$$

where N_s and N_p represents the number of series- and parallel-connected PV cells, respectively. It is evident from the Eq. (4) that the single diode model requires the determination of five unknown parameters—namely, I_{pv}, I_o, a, R_s, R_{sh}, which characterize the *I-V* curve.

2.2. Two-diode model

Although the single diode model offers a good compromise between simplicity and accuracy, it does not account for the effects of recombination current loss in the space charge region of the *p-n* junction. The consideration of this loss lead to a more elaborate model, known as the two-diode model (Chin et al., 2016). As shown in Fig. 2, it includes an additional diode connected in parallel to the first. The second diode accounts for the recombination current loss in the space charge region of the *p-n* junction. Following KCL, the current-voltage (*I-V*) relationship for the two-diode model can be written as,

$$I = I_{pv} - I_{d1} - I_{d2} - I_{sh} \tag{5}$$

where I_{d1} and I_{d2} are the current flowing through the first and second diodes, respectively. As with the single-diode model, they are defined by the Shockley's diode equations, given by,

$$I_{d1} = I_o\left(e^{\frac{V+IR_s}{a_1V_t}} - 1\right);\ \ I_{d2} = I_o\left(e^{\frac{V+IR_s}{a_2V_t}} - 1\right) \tag{6}$$

Hence, the current output of the two-diode model for a connection of PV cells can be written as,

$$I = I_{pv}N_p - I_{o1}N_p\left(e^{\frac{V+IR_s(N_s/N_p)}{a_1V_t}} - 1\right) - I_{o2}N_p\left(e^{\frac{V+IR_s(N_s/N_p)}{a_2V_t}} - 1\right) - \frac{V + IR_s(N_s/N_p)}{R_{sh}(N_s/N_p)} \tag{7}$$

where I_{o1} and I_{o2} are the saturation currents due to the diffusion mechanism and carrier recombination in the space-charge region, respectively. a_1 and a_2 are the ideality factors of the corresponding diodes. Thus, for the case of the two-diode model, the number of unknown parameters is seven, i.e. I_{pv}, I_{o1}, I_{o2}, a_1, a_2, R_s, R_{sh}. Additionally, due to the presence of two exponential terms, this model is substantially more complex than its single-diode counterpart. Nonetheless, it remains an appealing option due to its enhanced accuracy at low irradiance conditions (Chin et al., 2015a, 2016; Chin et al., 2017).

3. Objective function formulation

To effectively utilize EA for the parameter extraction problem, it is imperative to first define an appropriate objective function. Based on the premise that the most accurate set of model parameters should provide the closest fit to the experimental data, the optimal solution can be found by minimizing the difference between the computed and experimental data. In that regard, the widely accepted scheme to quantify the difference between two *I-V* curves is by the root mean square error (RMSE) (El-Naggar et al., 2012; Gao et al., 2018; Jiang et al., 2013; Oliva et al., 2017a; Zagrouba et al., 2010). Thus, the objective function can be defined as,

$$J(x) = RMSE = \sqrt{\frac{1}{N}\sum_{i=1}^{N}\left(I_{\exp}^{i} - I_{cal}^{i}(V_{\exp}^{i}, x)\right)^{2}} \tag{8}$$

where N denotes the number of experimental data points. I_{exp}^{i} and V_{exp}^{i} are the current and voltage values of the i-th empirical point, respectively. The variable x signifies the decision parameters of the optimization problem. Conversely, $I_{cal}^{i}(V_{\exp}^{i}, x)$ is the computed current output, where $x = [I_{pv}, I_o, a, R_s, R_{sh}]$ for the single diode model and $x = [I_{pv}, I_{o1}, I_{o2}, a_1, a_2, R_s, R_{sh}]$ for the two-diode model.

4. Coyote optimization algorithm

The Coyote Optimization Algorithm (COA) is a powerful population-based algorithm recently proposed by Juliano and Leandro (Coelho, 2018). The algorithm draws inspiration from the social behaviours of the *Canis latrans* species, which inhabits mainly the North America (Bekoff, 1977; Conner et al., 2008). Due to its unique structure, COA can be classified as both swarm intelligence and evolutionary heuristics. The population of coyotes is partitioned into N_p packs, with N_c coyotes per pack. The number of coyotes in each pack are assumed to be equal and constant. As such, the population size can be defined as the multiplication of N_p and N_c. The social conditions of each coyote signify a candidate solution $\vec{x}$ to the optimization problem. In that regard, the social conditions of the c^{th} coyote in the p^{th} pack at t^{th} time, is defined as,

$$soc_c^{p,t} = \vec{x} = (x_1, x_2. \ldots, x_D) \tag{9}$$

where D denotes the number of dimensions in the search space.

In the first step of COA, a population of $N_p \times N_c$ coyotes are initialized randomly within the predefined search space, given by,

$$soc_{c,j}^{p,t} = lb_j + r_j \cdot (ub_j - lb_j) \tag{10}$$

where lb and ub are the lower and upper bounds of the j^{th} decision parameter, respectively. r_j is a real number randomly generated between 0 and 1, following a uniform distribution. Subsequently, the adaptation of the coyotes to their respective social conditions are evaluated as follows,

$$fit_c^{p,t} = f(soc_c^{p,t}). \tag{11}$$

As observed in (Conner et al., 2008; Pitt et al., 2003), the coyotes have a tendency to leave their current packs to lead a solitary life, or join another pack. The expulsion of a coyote from its pack follows a probability P_e, which varies depending on the pack size:

$$P_e = 0.005 \cdot N_c^2. \tag{12}$$

This mechanism enhances population diversity by promoting global exchange of information among the coyote packs. Since P_e exceeds 1 for $N_c \geq \sqrt{200}$, COA limits the maximum number of coyotes per pack to 14.

In each pack, the coyote that is best accustomed to the environment is assigned as the alpha. For a minimization problem, the alpha can be determined by

$$alpha^{p,t} = \{soc_c^{p,t} | \arg_c = \{1, 2, \ldots, N_c\} \min f(soc_c^{p,t})\}. \tag{13}$$

By considering the obvious signs of swarm intelligence in coyotes, COA assumes each coyote shares its social conditions with the rest of the pack to improve the pack's survivability. In that regard, the cultural tendency of a pack is defined based on the information provided its members, i.e.

$$cult_j^{p,t} = \begin{cases} O_{\frac{(Nc+1)}{2}j}^{p,t}, & N_c \text{ is odd} \\ \dfrac{O_{\frac{Nc}{2}j}^{p,t} + O_{\frac{(Nc+1)}{2}j}^{p,t}}{2}, & \text{otherwise} \end{cases} \tag{14}$$

where $O^{p,t}$ denotes the ranked social conditions of the coyotes within p^{th} pack at the t^{th} time instance, for $j = 1,2\ldots D$. In this way, the cultural tendency of each pack is computed as the median of the collective social conditions within the pack.

In order to model the two major biological events of the coyotes, i.e. birth and death, the age of each coyote is considered, $age \in \mathbb{N}$. The birth of new coyotes is described as the amalgamation between the social conditions of two random parent coyotes from the same pack, and the influence of environmental factors R_j,

$$pup_j^{p,t} = \begin{cases} soc_{r1,j}^{p,t}, & rand_j < P_a \text{ or } j = j_1 \\ soc_{r2,j}^{p,t}, & rand_j < P_s + P_a \text{ or } j = j_2 \\ R_j, & \text{otherwise} \end{cases} \tag{15}$$

where $soc_{r1,j}^{p,t}$ and $soc_{r2,j}^{p,t}$ are random coyotes from the p^{th} pack, and j_1 and j_2 are two random dimensions of the search space. On the other hand, P_s and P_a are the scatter and association probabilities, respectively. R_j is a randomly generated vector within the bounds of the j^{th} dimension, and $rand_j$ is a uniform random number within the range [0.1]. The scatter and association probabilities have considerable influence on the diversity and composition of the coyote packs. Their values are defined as,

$$P_s = \frac{1}{D} \tag{16}$$

and

$$P_a = (1 - P_s)/2. \tag{17}$$

According to (Conner et al., 2008), the coyote pups has approximately 10% chances of dying at birth. Furthermore, the mortality risk of each coyote increases with age (Pitt et al., 2003). Therefore, COA models the coyotes' survivability based on a simple mechanism illustrated in Fig. 3; where ω and φ denote the group of coyotes less adjusted to the environment (i.e. worse fitness value) than the pup, and the size of the group, respectively. If two or more coyotes in the group are similar in age (line 4), the least adjusted will perish.

In addition, COA depicts the cultural interaction between the coyotes in the packs utilizing δ_1 and δ_2. The former refers to the influence of the alpha on a random coyote cr_1, while the latter signifies the influence of the cultural tendency of the pack on another random coyote cr_2. Both cr_1 and cr_2 are selected following a uniform distribution probability. Thus, δ_1 and δ_2 can be written as,

Algorithm 1 Birth and death of coyotes within a pack

1: Calculate ω and ϕ.
2: **if** $\phi = 1$ **then**
3: Retain the pup and eliminate the only coyote in ω.
4: **elseif** $\phi > 1$ **then**
5: Retain the pup and eliminate the oldest coyote in ω.
6: **else**
7: Eliminate the pup.
8: **end if**

Fig. 3. Pseudocode for the birth and death of coyotes within a pack.

$$\delta_1 = alpha^{p,t} - soc_{cr1}^{p,t} \quad (18)$$

and

$$\delta_2 = cult^{p,t} - soc_{cr2}^{p,t}. \quad (19)$$

The social conditions of the coyotes are influenced by both the alpha and other members of the pack. In COA, they are updated by the following equation,

$$new\_soc_c^{p,t} = soc_c^{p,t} + r_1 \cdot \delta_1 + r_2 \cdot \delta_2 \quad (20)$$

where r_1 and r_2 are uniformly generated random values within the range [0,1]. The new social conditions of the coyotes are evaluated using,

$$new\_fit_c^{p,t} = f(new\_soc_c^{p,t}). \quad (21)$$

By virtue of their excellent cognitive abilities, the coyotes can then decide to keep the new social conditions if any improvement is perceived over the previous. Otherwise, the latter will be retained. In other words, the overall fitness of the coyotes will either improve or stay the same, but never worsen.

$$soc_c^{p,t+1} = \begin{cases} new\_soc_c^{p,t}, & \text{if } new\_fit_c^{p,t} < fit_c^{p,t} \\ soc_c^{p,t}, & \text{otherwise} \end{cases}. \quad (22)$$

4.1. Parameter constraints

A potential issue with the implementation of Eq. (20) for the parameter extraction of solar cells is that it could cause the coyotes (i.e. the model parameters) to stray outside of the predefined search boundaries and yield physically unrealistic solutions. In this work, a simple operator as shown in Eq. (23) is introduced to prevent such occurrence. Following this constraint, the violating elements are re-initialized randomly within the search space,

$$new\_soc_{c,j}^{p,t} = \begin{cases} lb_j + rand_j(ub_j - lb_j), & \text{if } new\_soc_{c,j}^{p,t} < lb_j \text{ or } new\_soc_{c,j}^{p,t} \\ & > ub_j \\ new\_soc_{c,j}^{p,t}, & \text{otherwise} \end{cases}. \quad (23)$$

Fig. 4 presents a summary of COA in the form of pseudo-code. The algorithm is reiterated until a predefined stopping criterion—normally a fitness threshold or a maximum generation count (Gen_{max}), is met. The coyote that is best adjusted to the environment (i.e. with the best fitness) is chosen as the global optimum solution.

5. Experimental results

To investigate the performance of the COA-based optimizer, it is implemented in MATLAB to extract the parameters of the single diode and two-diode models. For comparison with other relevant works, two sets of *I-V* data—namely, the measurements acquired from the R.T.C France 57 mm diameter silicon solar cell and the Photowatt-PWP 201 polycrystalline module, are utilized (Easwarakhanthan et al., 1986). These datasets are chosen because they have been widely utilized as benchmarks to evaluate the performances of numerous parameter extraction methods (Abd Elaziz and Oliva, 2018; Askarzadeh and Rezazadeh, 2012, 2013a; Chen et al., 2018; Chen et al., 2016a; Chen et al., 2016b; Gao et al., 2018; Gong and Cai, 2013; Guo et al., 2016; Hachana et al., 2013; Han et al., 2014; Jamadi et al., 2016; Kler et al., 2017; Lin et al., 2017; Oliva et al., 2017a; Oliva et al., 2014; Oliva et al., 2017b; Wei et al., 2011; Wu et al., 2018; Xu and Wang, 2017; Yu et al., 2018b; Zhang et al., 2016). The exact value of each data points and the best results obtained by other methods are readily available in the literature. Thus, these case studies provide fair, wide-reaching, and referenceable comparisons. The parameters search ranges are set according to other related works (Askarzadeh and Rezazadeh, 2013a; Gao et al., 2018; Guo et al., 2016), as shown in Table 1. Additionally, to further demonstrate the practicality of the algorithm, it is tested on three commercial modules of different PV technologies, namely, SM55 (mono-crystalline), RSM50 (poly-crystalline), and ST40 (thin film), at varying environmental conditions. The experiments are performed on a computer with Intel Core i7-4790 3.60 GHz processor, 16 GB RAM and Windows 10 Home 64-bit operating system.

5.1. Setting the control parameters

For effective implementation of COA, the control parameters must be set properly. A major advantage of COA is that it only requires the tuning of two control parameters, i.e. N_p and N_c. While there is no strict guideline in selecting these values, it is recommended that N_c can be first set within [5,10], then N_p can be adjusted accordingly to define the

Algorithm 2 Overall pseudo-code of COA

```
Generate N_p packs, with N_c coyotes each (Eqn. 10).
Assess each coyote's adaptation (Eqn. 11).
while stopping criterion is unfulfilled do
    for each p pack do
        Determine the alpha of the pack (Eqn. 13).
        Calculate the social tendency of the pack (Eqn. 14).
            for each coyote c of the pack p do
                Generate new social conditions (Eqn. 20).
                Check boundary conditions (Eqn. 23)
                Evaluate the new social conditions (Eqn. 21).
                Decide whether to move or stay (Eqn. 22).
            end for
        Simulate the birth and death of coyotes (Eqn. 15 and Alg. 1).
    end for
    Impose the probabilities of coyotes leaving their packs (Eqn. 12).
    Update the ages of the coyotes.
endwhile
Choose the coyote best adapted to the environment.
```

Fig. 4. The overall pseudo-code of COA.

Table 1
Search boundaries of the model parameters.

Parameters	R.T.C France solar cell		Photowatt-PWP 201 module	
	Lower bound	Upper bound	Lower bound	Upper bound
I_{pv}	0	1	0	2
I_o, I_{o1}, I_{o2}	0	1	0	1
a, a_1, a_2	1	2	1	2
R_s	0	0.5	0	0.5
R_{sh}	0	100	0	100

Table 2
The average fitness obtained for the single diode model using different control parameters settings.

Settings	N_c	N_p	Population size	Average fitness
A	5	20	100	0.001289080
B	6	17	102	0.001137787
C	7	14	98	0.001124050
D	8	13	104	0.001102134
E	**9**	**11**	**99**	**0.001102101**
F	10	10	100	0.001228196

Table 3
The average fitness obtained for the two-diode model using different control parameters settings.

Settings	N_c	N_p	Population size	Average fitness
A	5	20	100	0.001500542
B	**6**	**17**	**102**	**0.001370024**
C	7	14	98	0.001490444
D	8	13	104	0.001808610
E	9	11	99	0.002416901
F	10	10	100	0.002843153

total population size ($N_c \times N_p$) (Coelho, 2018). In this subsection, a systematic procedure is utilized to determine the optimal control parameter settings for the parameter extraction problem. To this end, the experimental dataset presented in Table 5 is used as an example.

By varying N_c from 5 to 10, the corresponding value of N_p is adjusted to approximate a total population size of 100, as shown in Table 2 and 3. Note that, since N_c = 6, 7, 8, and 9 (for settings B, C, D and E, respectively) are not factors of 100, the corresponding values of N_p are rounded up to the closest integers. This results in variations in population sizes within ± 4 of 100; which is negligible. For each setting, the algorithm is allowed 500 iterations and is executed for 50 independent runs. The average RMSE obtained for the single diode and two-diode models are tabulated in Table 2 and Table 3, respectively. It can be inferred from Table 2 that, setting E yields best performance for the single diode model. Specifically, it converges to a RMSE value of 1.10210E-3 A. This is a considerable contrast in comparison to the worst performer, i.e. setting A, which yields a RMSE value of 1.28908E-3 A. As for the two-diode model, the best performance is achieved by employing setting B, as shown in Table 3. Note that the fitness value obtained by setting B, i.e. RMSE = 1.37002E-3 A, is more than two times lower than that of setting F (average fitness = 2.84315E-3 A). Although these findings clearly demonstrate the importance of selecting the appropriate control parameters for COA, it should be clarified that fitness values shown here are by no means the optimum solutions. The actual work on the parameter extraction problem is discussed in the subsequent subsections. In view of these results, this work employs setting E (N_c = 9, N_p = 11) for the single diode model, and setting B (N_c = 6, N_p = 17) for the two-diode model. The maximum number of iterations ($iter_{max}$) is set to 10,000.

5.2. Comparison with other relevant works

5.2.1. Accuracy for the single diode model

In the first case study, the COA is utilized to identify the parameters of the single diode model for the 57-mm diameter R.T.C. France commercial silicon solar cell (Easwarakhanthan et al., 1986). The experimental data contains 26 pairs of *I-V* data points (N = 26) measured under 45 °C. The parameters obtained using the COA and other relevant works for the single diode model are shown in Table 4. The results indicate that COA outperformed its competitors by a considerable margin. In particular, the RMSE obtained by COA is 7.7301E−04 A; whereas the second-best solution, i.e. the 3-point-based method (Chin and Salam, 2019) has a RMSE value of 8.1291E-04 A. It is followed by MPCOA (Yuan et al., 2014), which achieved RMSE of 9.4457E−04 A. In comparison, the RMSEs of other state-of-the-art algorithms such as CWOA (Oliva et al., 2017a), TLABC (Chen et al., 2018), NM-MPSO (Hamid et al., 2016), OBWOA (Abd Elaziz and Oliva, 2018), EHA-NMS (Chen et al., 2016b), ABC-DE (Hachana et al., 2013), ABC-TRR (Wu et al., 2018), Rcr-IJADE (Gong and Cai, 2013), STLBO (Guo et al., 2016), ISCE (Gao et al., 2018), and CSO (Guo et al., 2016) are capped in the vicinity of 9.8602E − 04 A. On the other hand, BFA (Oliva et al., 2014) yielded the least accurate solutions, i.e. 0.029 A.

Table 5 provides a comparison between the experimental dataset and the *I-V* curve computed by COA. It is evident from the table that the absolute error is kept very low through the entire range of voltage. The mean absolute error (MAE) is observed to be only 0.000644 A. For visual validation, the extracted model parameters are utilized to reconstruct the *I-V* and *P-V* output of the single diode model, as shown in Fig. 5. As expected, the model is highly consistent with the experimental data throughout the entire range of voltage.

5.2.2. Accuracy for the two-diode model

This case study examines the performance of the COA for the parameter extraction of the two-diode model. As with the previous case, the dataset of the 57-mm diameter R.T.C. France commercial silicon solar cell is used (Easwarakhanthan et al., 1986). For comparison, the parameters values and RMSE obtained by the COA and other relevant works are presented in Table 6. Additionally, Table 5 provides a detailed comparison between the computed and experimental *I-V* data points. Meanwhile, the graphical validation of the results is as shown in Fig. 6. It can be observed from Table 6 that the COA computed the most accurate solution, i.e. the RMSE is only 7.3265E-04 A. As with previous case, the study in (Yuan et al., 2014) reported the second best results (RMSE = 9.2163E-04). It followed by STBLO (Guo et al., 2016) and DE/WOA (Xiong et al., 2018), which reported RMSEs of 9.82E-04 and 9.8248E-04, respectively.

By comparing the results given in Tables 4 and 6, it is interesting to observe that the two-diode model is in general more accurate than its single diode counterpart, regardless of the choice of optimization algorithm. This observation agrees well with the findings reported elsewhere (Chin et al., 2017; Hasan and Parida, 2016). Nonetheless, note that the fitting accuracy achieved by COA using the single diode model (i.e. RMSE = 7.7301E−04 A), surpasses even the best results reported by other works for the two-diode model.

On the other hand, for the sake of interest, the parameter extraction method is also implemented to extract the parameters of the ideal model. As its name suggests, the latter depicts the ideal characteristics of the cell, i.e. in the absence of the losses that are incurred in a practical solar cell. Therefore, it is essentially the single diode model with the absence of both series and shunt resistances (x = [I_{pv}, I_o, a]). The model equation and its topology are not produced here for brevity.

Table 4
The extracted parameters and their fitting accuracies for the 57-mm diameter R.T.C. France commercial silicon solar cell using the single diode model.

Method	I_{pv}	I_o (μ)	a	R_s	R_{sh}	RMSE
COA	0.760788	0.31069	1.47727	0.03655	52.8898	7.7301E−04
3-point-based (DE) (Chin and Salam, 2019)	0.76072	0.31911	1.47986	0.03629	54.19241	8.1291E-04
MPCOA (Yuan et al., 2014)	0.76073	0.32655	1.48168	0.03635	54.6328	9.4457E−04
CWOA (Oliva et al., 2017a)	0.76077	0.3239	1.4812	0.03636	53.7987	9.8602E−04
TLABC (Chen et al., 2018)	0.76078	0.32302	1.48118	0.03638	53.7164	9.8602E−04
NM-MPSO (Hamid et al., 2016)	0.76078	0.32306	1.4812	0.03638	53.7222	9.8602E−04
OBWOA (Abd Elaziz and Oliva, 2018)	0.76077	0.3232	1.5208	0.0363	53.6836	9.8602E−04
EHA-NMS (Chen et al., 2016b)	0.760776	0.32302	1.48118	0.03638	53.7185	9.8602E−04
ABC-DE (Hachana et al., 2013)	0.76077	0.32302	1.47986	0.03637	53.7185	9.8602E−04
ABC-TRR (Wu et al., 2018)	0.760776	0.32302	1.48118	0.03638	53.7185	9.8602E−04
Rcr-IJADE (Gong and Cai, 2013)	0.760776	0.32302	1.48118	0.03638	53.7185	9.8602E−04
STLBO (Guo et al., 2016)	0.76078	0.32302	1.48114	0.03638	53.7187	9.8602E−04
ISCE (Gao et al., 2018)	0.760776	0.32302	1.48118	0.03638	53.7185	9.8602E−04
CSO (Guo et al., 2016)	0.76078	0.323	1.48118	0.03638	53.7185	9.8602E−04
HFAPS (Beigi and Maroosi, 2018)	0.760777	0.32262	1.48106	0.03638	53.6784	9.8602E-04
DE/WOA (Xiong et al., 2018)	0.760776	0.32302	1.48118	0.03638	53.7185	9.8602E−04
ILCOA (Pourmousa et al., 2019)	0.76078	0.32302	1.48111	0.03638	53.7187	9.8602E−04
LCOA (Pourmousa et al., 2019)	0.76075	0.32328	1.48119	0.03637	53.9024	9.8609E−04
LMSA (Dkhichi et al., 2014)	0.7608	0.3185	1.4798	0.0364	53.3264	9.86E−04
PCE (Zhang et al., 2016)	0.760776	0.323021	1.481074	0.03638	53.7185	9.8602E−04
PSO (Hamid et al., 2016)	0.76077	0.32454	1.48165	0.03636	53.8550	9.8606E−04
BMO (Askarzadeh and Rezazadeh, 2013b)	0.76077	0.32479	1.48173	0.03636	53.8716	9.8608E−04
MABC (Jamadi et al., 2016)	0.760779	0.321323	1.481385	0.03639	53.4000	9.8610E−04
ABC (Oliva et al., 2014)	0.7608	0.3251	1.4817	0.0364	53.6433	9.8620E−04
GOTLBO (Chen et al., 2016a)	0.76078	0.331552	1.48382	0.03627	54.1154	9.8744E−04
GGHS (Askarzadeh and Rezazadeh, 2012)	0.76092	0.3262	1.48217	0.03631	53.0647	9.9097E−04
ABSO (Askarzadeh and Rezazadeh, 2013a)	0.7608	0.30623	1.47583	0.03659	52.2903	9.9124E−04
IGHS (Askarzadeh and Rezazadeh, 2012)	0.76077	0.34351	1.4874	0.03613	53.2845	9.9306E−04
HS (Askarzadeh and Rezazadeh, 2012)	0.7607	0.305	1.4754	0.0366	53.5946	9.95E−04
CPSO (Wei et al., 2011)	0.7607	0.4	1.5033	0.0354	59.012	1.3900E−03
Newton (Easwarakhanthan et al., 1986)	0.7608	0.3223	1.4837	0.0364	53.7634	9.70E−03
PS (AlHajri et al., 2012)	0.7617	0.998	1.6	0.0313	64.1026	0.0149
SA (El-Naggar et al., 2012)	0.762	0.4798	1.5172	0.0345	43.1034	0.019
GA (Oliva et al., 2014)	0.7619	0.8087	1.5751	0.0299	42.3729	0.019
BFA (Oliva et al., 2014)	0.7602	0.8000	1.6951	0.0325	50.8691	0.029

Table 5
The absolute error between the computed current and the experimental data of the single diode and two-diode models for the 57-mm diameter R.T.C. France commercial silicon solar cell.

Data point	V_{exp} (V)	I_{exp} (A)	Single-diode model			Two-diode model		
			I_{cal} (A)	Absolute power error (W)	Absolute current error (A)	I_{cal} (A)	Absolute power error (W)	Absolute current error (A)
1	−0.2057	0.764	0.7641	0.0000	0.0001	0.7638	0.0000	0.0002
2	−0.1291	0.762	0.7627	0.0001	0.0007	0.7625	0.0001	0.0005
3	−0.0588	0.7605	0.7614	0.0001	0.0009	0.7613	0.0000	0.0008
4	0.0057	0.7605	0.7602	0.0000	0.0003	0.7602	0.0000	0.0003
5	0.0646	0.76	0.7590	0.0001	0.0010	0.7592	0.0001	0.0008
6	0.1185	0.759	0.7580	0.0001	0.0010	0.7583	0.0001	0.0007
7	0.1678	0.757	0.7570	0.0000	0.0000	0.7573	0.0001	0.0003
8	0.2132	0.757	0.7561	0.0002	0.0009	0.7564	0.0001	0.0006
9	0.2545	0.7555	0.7550	0.0001	0.0005	0.7553	0.0001	0.0002
10	0.2924	0.754	0.7536	0.0001	0.0004	0.7538	0.0001	0.0002
11	0.3269	0.7505	0.7513	0.0003	0.0008	0.7513	0.0003	0.0008
12	0.3585	0.7465	0.7473	0.0003	0.0008	0.7471	0.0002	0.0006
13	0.3873	0.7385	0.7401	0.0006	0.0016	0.7397	0.0005	0.0012
14	0.4137	0.728	0.7274	0.0002	0.0006	0.7270	0.0004	0.0010
15	0.4373	0.7065	0.7070	0.0002	0.0005	0.7067	0.0001	0.0002
16	0.459	0.6755	0.6754	0.0000	0.0001	0.6753	0.0001	0.0002
17	0.4784	0.632	0.6310	0.0005	0.0010	0.6311	0.0004	0.0009
18	0.496	0.573	0.5722	0.0004	0.0008	0.5725	0.0003	0.0005
19	0.5119	0.499	0.4995	0.0003	0.0005	0.4998	0.0004	0.0008
20	0.5265	0.413	0.4135	0.0003	0.0005	0.4137	0.0004	0.0007
21	0.5398	0.3165	0.3172	0.0004	0.0007	0.3172	0.0004	0.0007
22	0.5521	0.212	0.2120	0.0000	0.0000	0.2118	0.0001	0.0002
23	0.5633	0.1035	0.1026	0.0005	0.0009	0.1024	0.0006	0.0011
24	0.5736	−0.0100	−0.0093	0.0004	0.0007	−0.0095	0.0003	0.0005
25	0.5833	−0.1230	−0.1244	0.0008	0.0014	−0.1244	0.0008	0.0014
26	0.59	−0.2100	−0.2091	0.0005	0.0009	−0.2088	0.0007	0.0012
Sum of AE					0.017633			0.016751
MAE					0.000678			0.000644
RMSE (fitness value)					7.730064E-04			7.326481E-04

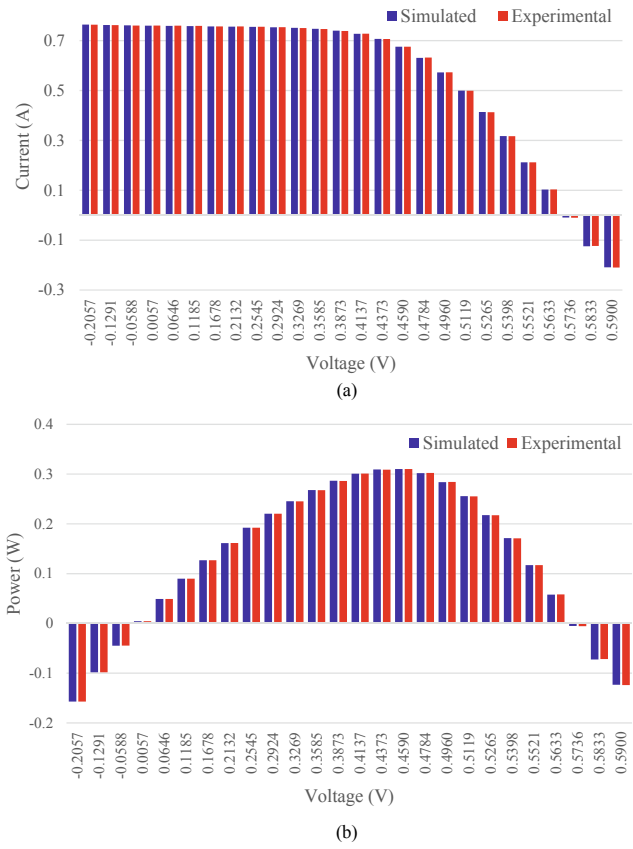

Fig. 5. Comparison between the computed output and empirical data of the 57-mm diameter R.T.C. France commercial silicon solar cell for the single diode model: (a) *I-V* curve data (b) *P-V* curve data.

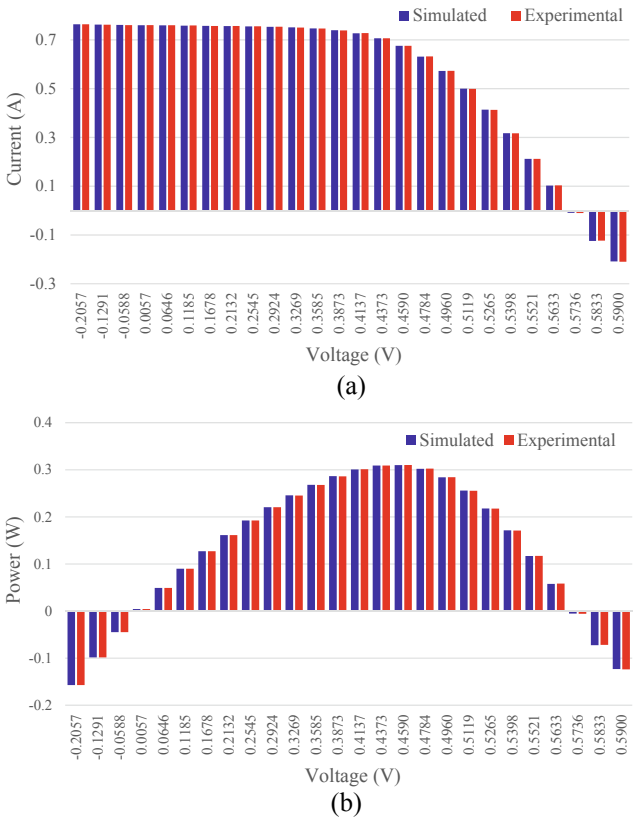

Fig. 6. Comparison between the computed output and empirical data of the 57-mm diameter R.T.C. France commercial silicon solar cell for the two-diode model: (a) *I-V* curve data (b) *P-V* curve data.

The extracted parameters are: I_{PV} = 0.753329, I_o = 1.4243E-05, a = 2. Fig. 7 depicts the comparison between the simulated and experimental curves. In addition, a brief comparison of the results in terms of RMSE is provided in Table 7. While it is clear that the omittance of R_s and R_p greatly simplifies the computation, it has an adverse effect on the fitness accuracy. In particular, the RMSE of the ideal model is observed to be more than one order of magnitude poorer than the other two models. It is therefore not advisable to employ this model for applications where highly accurate solutions are required.

5.2.3. Accuracy for the PV module

In this case study, the parameter extraction for the Photowatt-PWP 201 module is examined. The module comprises 36 polycrystalline series-connected poly-crystalline cells. For comparison with other relevant works, the COA is employed to determine the parameters of the single diode model. The experimental dataset has 25 pairs of *I-V* data points, which was measured under $G = 1000\,W/m^2$ and $T = 45\,^{\circ}C$. Table 8 shows a comprehensive comparison between the results obtained by COA and that of other relevant works. Further, the point-by-point assessment between the experimental data points and the curve computed by COA is given in Table 9. As with the previous cases, the parameters values obtained by COA are comparable those reported in

Table 6
The extracted parameters and their fitting accuracies for the 57-mm diameter R.T.C. France commercial silicon solar cell using the two-diode model.

Method	I_{pv}	I_{o1} (μ)	I_{o2} (μ)	a_1	a_2	R_s	R_{sh}	RMSE
COA	0.76081	0.08656	0.21597	1.37278	2.00000	0.03803	58.3562	7.3265E-04
MPCOA (Yuan et al., 2014)	0.76078	0.31259	0.04528	1.47844	1.78459	0.03635	54.2531	9.2163E-04
STBLO (Guo et al., 2016)	0.76078	0.22566	0.75217	1.45085	2	0.03674	55.492	9.82E-04
DE/WOA (Xiong et al., 2018)	0.76078	0.22597	0.74935	1.45102	2	0.03674	55.4854	9.8248E-04
HFAPS (Beigi and Maroosi, 2018)	0.76078	0.22597	0.74936	1.45101	2	0.03674	55.4855	9.8248E-04
OBWOA (Abd Elaziz and Oliva, 2018)	0.76076	0.2299	0.61956	1.49154	2	0.03671	55.399	9.8251E-04
ILCOA (Pourmousa et al., 2019)	0.76078	0.22601	0.74921	1.45101	2	0.03674	55.5320	9.8257E−04
CWOA (Oliva et al., 2017a)	0.76077	0.2415	0.6	1.45651	1.9899	0.03666	55.2016	9.8272E-04
BMO (Askarzadeh and Rezazadeh, 2013b)	0.76078	0.2111	0.87688	1.44533	1.99997	0.03682	55.8081	9.83E-04
ABSO (Askarzadeh and Rezazadeh, 2013a)	0.76078	0.26713	0.38191	1.46512	1.98152	0.03657	54.6219	9.83E-04
CSO (Guo et al., 2016)	0.76078	0.22732	0.72785	1.45151	1.99769	0.03674	55.3813	9.83E-04
LCOA (Pourmousa et al., 2019)	0.76077	0.26612	0.38023	1.46205	1.9938	0.3667	54.6314	9.8423E-04
IGHS (Askarzadeh and Rezazadeh, 2012)	0.76079	0.9731	0.16791	1.92126	1.42814	0.0369	56.8368	9.86E-04
HS (Askarzadeh and Rezazadeh, 2012)	0.76176	0.12545	0.2547	1.49439	1.49989	0.03545	46.82696	0.00126
GGHS (Askarzadeh and Rezazadeh, 2012)	0.76056	0.37014	0.13504	1.49638	1.92998	0.03562	62.7899	0.00107
PS (AlHajri et al., 2012)	0.7602	0.9889	0.0001	1.6	1.192	0.032	81.3008	0.01518
SA (El-Naggar et al., 2012)	0.7623	0.4767	0.01	1.5172	2	0.0345	43.1034	0.01664

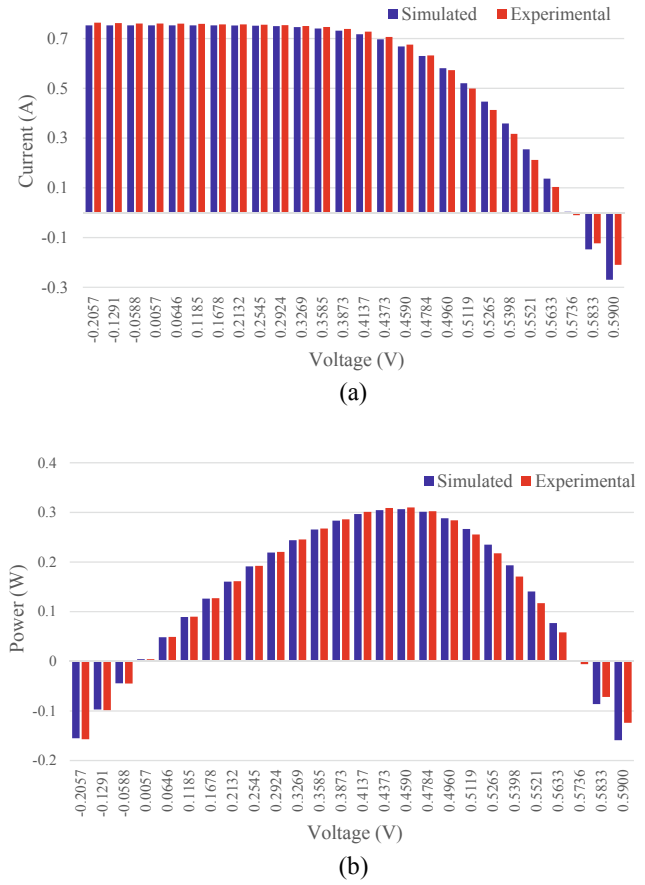

Fig. 7. Comparison between the computed output and empirical data of the 57-mm diameter R.T.C. France commercial silicon solar cell for the ideal model: (a) *I-V* curve data (b) *P-V* curve data.

Table 7
Comparison of fitting accuracy obtained for different models of the solar cell.

Model	Accuracy (RMSE)
Single-diode model	7.7301E−04
Two-diode model	7.3265E-04
Ideal diode model	2.0991E−02

Table 9
The absolute error between the computed current and the experimental data for Photowatt-PWP 201 polycrystalline PV module.

Data point	V_{exp} (V)	I_{exp} (A)	I_{cal} (A)	Absolute power error (W)	Absolute current error (A)
1	0.1248	1.0315	1.0297	0.00022	0.0018
2	1.8093	1.03	1.0277	0.00423	0.0023
3	3.3511	1.026	1.0257	0.00092	0.0003
4	4.7622	1.022	1.0238	0.00873	0.0018
5	6.0538	1.018	1.0218	0.02309	0.0038
6	7.2364	1.0155	1.0193	0.02767	0.0038
7	8.3189	1.014	1.0157	0.01442	0.0017
8	9.3097	1.01	1.0100	0.00020	0.0000
9	10.2163	1.0035	1.0004	0.03157	0.0031
10	11.0449	0.988	0.9847	0.03598	0.0033
11	11.8018	0.963	0.9602	0.03318	0.0028
12	12.4929	0.9255	0.9239	0.02032	0.0016
13	13.1231	0.8725	0.8736	0.01400	0.0011
14	13.6983	0.8075	0.8082	0.00963	0.0007
15	14.2221	0.7265	0.7286	0.02916	0.0021
16	14.6995	0.6345	0.6366	0.03136	0.0021
17	15.1346	0.5345	0.5354	0.01405	0.0009
18	15.5311	0.4275	0.4282	0.01086	0.0007
19	15.8929	0.3185	0.3179	0.01033	0.0006
20	16.2229	0.2085	0.2070	0.02420	0.0015
21	16.5241	0.101	0.0976	0.05545	0.0034
22	16.7987	−0.008	−0.0086	0.00989	0.0006
23	17.0499	−0.111	−0.1110	0.00048	0.0000
24	17.2793	−0.209	−0.2086	0.00679	0.0004
25	17.4885	−0.303	−0.3009	0.03625	0.0021
Sum of AE					0.04255774
MAE					0.00170231
RMSE (fitness value)					2.052961E−03

other works. However, upon close inspection on the RMSE values, it is clear that the solution given by the COA is the most accurate (RMSE = 2.052961E−03), followed by the 3-point-based method (Chin and Salam, 2019), TLABC (Chen et al., 2018), DE/WOA (Xiong et al., 2018), HFAPS (Beigi and Maroosi, 2018), Rcr-IJADE (Gong and Cai, 2013), EHA-NMS (Chen et al., 2016b). Conversely, the RMSE error recorded by the Newton method (Easwarakhanthan et al., 1986) is up to two orders of magnitude worse than its metaheuristic counterparts. For better insights, Fig. 8 presents visual comparisons of the PV model outputs with the experimental data. As expected, the model is in excellent agreement with the experimental data for all values of voltage. The MAE of the computed *I-V* curve is only 0.00170231A.

Table 8
The extracted parameters and their fitting accuracies for Photowatt-PWP 201 polycrystalline PV module.

Method	I_{pv}	I_o (μ)	a	R_s	R_{sh}	RMSE
Proposed method	1.03143	2.63808	1.32217	0.03432	22.82338	2.052961E−03
3-point-based (DE) (Chin and Salam, 2019)	1.03353	2.12479	1.30017	0.03471	19.37196	2.422747E-03
TLABC (Chen et al., 2018)	1.03056	3.4715	1.35087	0.03338	27.02599	2.42507E−03
DE/WOA (Xiong et al., 2018)	1.03051	3.48226	1.35119	0.03337	27.27728	2.425075E−03
HFAPS (Beigi and Maroosi, 2018)	1.03051	3.48226	1.35125	0.03337	27.34115	2.4251E-03
Rcr-IJADE (Gong and Cai, 2013)	1.03051	3.48226	1.35119	0.03337	27.27728	2.425075E−03
EHA-NMS (Chen et al., 2016b)	1.03051	3.48226	1.35119	0.03337	27.27728	2.425075E−03
ISCE (Gao et al., 2018)	1.03051	3.48226	1.35119	0.03337	27.27729	2.425075E−03
ABC-TRR (Wu et al., 2018)	1.03051	3.48226	1.35119	0.03337	27.27728	2.425E−03
MPCOA (Yuan et al., 2014)	1.03188	3.37370	1.34740	0.03342	23.60258	2.4251E−03
FPA (Alam et al., 2015)	1.03209	3.04754	1.33698	0.03382	22.53811	2.7425E−03
ABC-DE (Hachana et al., 2013)	1.0318	3.2774	1.3443	0.03351	23.47915	3.8855E−03
Newton (Easwarakhanthan et al., 1986)	1.0318	3.2876	1.34583	0.03349	15.26250	5.6010E-01

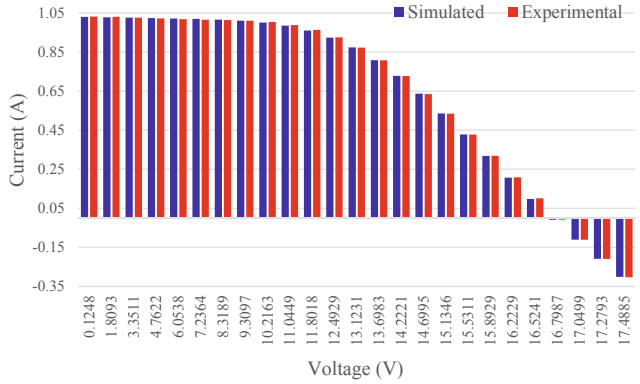

(a)

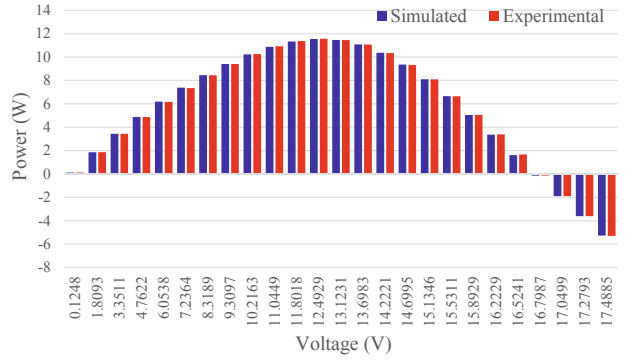

(b)

Fig. 8. Comparison between the computed output and empirical data of Photowatt-PWP 201 PV module for the single diode model: (a) *I-V* curve data (b) *P-V* curve data.

5.3. Convergence rate

Fig. 9 presents the convergence profile of COA for all three cases discussed in Section 5.2. From the figure, it is evident that the optimizer requires relatively low number of iterations to identify the optimal solutions for the single diode model. Specifically, it successfully achieves stable convergence for the R.T.C France silicon solar cell and the Photowatts-PWP 201 module in 636 and 718 iterations, respectively. On the other hand, greater computation effort, i.e. 7677 iterations, is required to extract the parameters of the two-diode model. This is expected considering the two-diode model is structurally more complex and comprises greater number of parameters than its single diode counterpart. Nonetheless, it is remarkable to note that the COA surpasses the best fitness reported by other works (i.e. RMSE = 9.2163E-04) within only 402 iterations.

Table 10
Mean and STD of the fitness values over 35 independent runs.

Cases		Fitness
R.T.C France 57 mm diameter solar cell (single diode model)	Mean	7.730063E-04
	STD	1.909221E-17
R.T.C France 57 mm diameter solar cell (two-diode model)	Mean	7.331449E-04
	STD	2.898496E-06
Photowatt-PWP 201	Mean	2.052961E-03
	STD	1.912235E-17

Table 11
Comparison of RMSEs STD for the R.T.C France 57-mm diameter commercial silicon solar cell (Oliva et al., 2017a; Oliva et al., 2014).

Algorithm	STD of RMSE
COA	1.9092E-17
3-point-based (DE)	1.9106E-12
CWOA	1.0216E-08
STBLO	1.1333E-07
ABC	1.497E-05
BMO	3.986E-05
HS	0.7268
PSO	0.0289
GA	0.0735
BFA	0.0586

5.4. Consistency

In this section, the consistency of the COA-based optimizer is evaluated. The algorithm is executed for 35 instances, and the results are

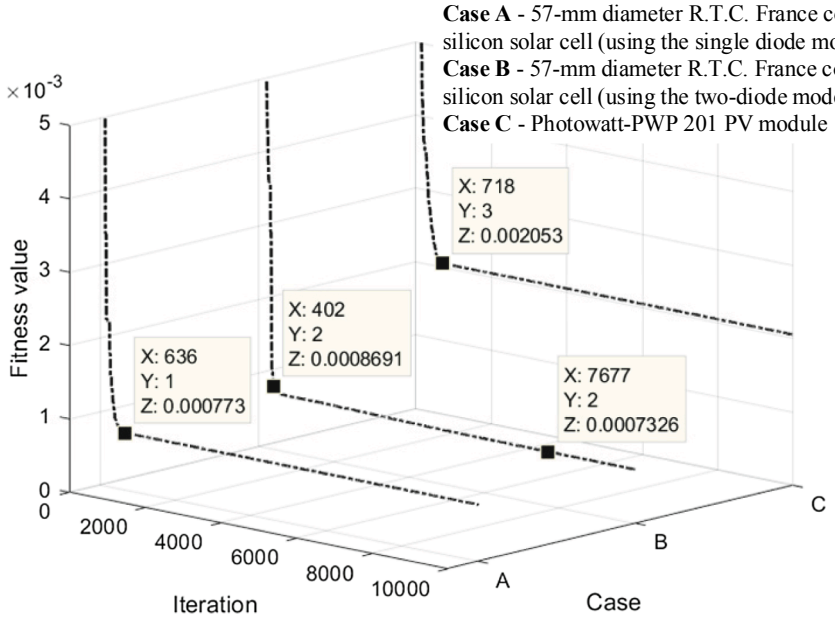

Fig. 9. Convergence profiles of the COA-based optimizer for different case studies.

Table 12
PV module specifications.

Parameters	Shell SM55 (Mono-crystalline)	Shell RSM50 (Poly-crystalline)	Shell ST40 (Thin film)
Short circuit current, I_{SC} (A)	3.45	3.1	2.68
Open circuit voltage, V_{OC} (V)	21.7	21.7	23.3
Peak power current, I_{MPP} (A)	3.15	2.82	2.41
Peak power voltage, V_{MPP} (V)	17.4	17	16.6
Short circuit current temperature coefficient, K_i (mA/°C)	1.40	1	0.35
Open circuit voltage temperature coefficient, K_v (mA/°C)	-α76.0	−78	−100
Number of cells in series, N_s	36	36	42

recorded. Table 10 shows the mean and standard deviation (STD) of the RMSE obtained. A low STD denotes most values are very close to the average, while high STD implies a more scattered pattern. In this context, the STD can be viewed as a stability index, which indicates the ability of the algorithm to produce comparable results when executed for multiple number of times. Table 10 reveals that the optimizer obtains lower STD for the single diode model than the two-diode model. This is to be expected as the former contains a smaller number of decision parameters—thus a more confined search space. Nonetheless, the STD is exceptionally low for all cases, i.e. less than 1×10^{-5}. These findings imply that the COA is very consistent; therefore, the optimal solution is almost always guaranteed.

For comparison, Table 11 presents the STD of the results obtained by COA and other EA-based optimizers for the 57 mm- diameter R.T.C France solar cell (Oliva et al., 2017a; Oliva et al., 2014). As with the COA, the latter are performed for 35 times and are allowed up to 10,000 iterations to calculate best possible solutions. From the results, it is evident that the COA offers vastly outperformed the others in terms of consistency. Particularly, the STD of COA is more than five order of magnitude lower compared to the competitors.

5.5. Parameters extraction at various environmental conditions

To further validate the practicality of the COA-based optimizer, the algorithm is utilized to extract the parameters of three different types of commercial PV modules at various environmental conditions. The selected modules are namely, the Shell SM55 (mono-crystalline), Shell RSM50 (poly-crystalline), and Shell ST40 (thin film), whose specifications are tabulated in Table 12. The experimental data points are extracted from the manufacturer datasheets of the PV modules. Fig. 10 presents the computed *I-V* curves and experimental data points for multiple irradiance and temperature variations. The parameters values extracted at these conditions are given in the Appendix A (Tables A1 and A2). Note that the asterisk in Table A1 indicates the *G* for RSM50 are given in brackets.

The figures show that the computed *I-V* curves are highly consistent with the empirical data, even at environmental conditions far from the Standard Test Conditions (STC)[1]. In particular, the RMSE of the model is less than 0.02 A for all cases. The accuracy of the model at high temperature and low irradiance conditions are especially crucial because PV systems typical operate under irradiance less than 1000 W/m^2 (Lorenz et al., 2009; Mellit and Pavan, 2010; Yang et al., 2014), while the module temperatures (especially for roof-mounted/back-insulated installations) could easily rise above 50 °C at midday (Davis et al., 2001; Kurtz et al., 2011; Poulek et al., 2018; Rajput et al., 2018; Strevel et al., 2012). Further, the modelling accuracy at low irradiances is essential for partial shading simulations (Mäki and Valkealahti, 2012). Additionally, it is worthwhile to note that the thin film module (ST40) acquires higher series resistance than the crystalline modules; which explains the lower efficiency of the former. This observation is consistent with the findings reported elsewhere (Chin et al., 2017; Ishaque et al., 2012). Besides, PV modules are known to exhibit high shunt resistance and low series resistance values (Chin and Salam, 2018; Villalva et al., 2009). These attributes are clearly demonstrated in the extracted parameters values.

[1] STC is the industry standard conditions for testing the performance of PV modules. It refers to solar irradiance of 1000 W/m^{2,} with 1.5 air mass and temperature at 25 °C.

6. Conclusion

In this work, the COA is implemented for the parameter extraction of PV cell models. The algorithm offers a unique computation structure that promotes a good balance between exploration and exploitation. Moreover, the algorithm has only two control parameters, i.e. N_c and N_p. Thus, it is simple to implement and does not require laborious trial-and-errors effort to determine the optimum settings. To ensure a physically meaningful solution is obtained, a set of parametric constraints is utilized to discard out-of-bound vectors. Despite its simplicity, it was proven that the COA outperformed other recent metaheuristic algorithms, such as the MPCOA, DE/WOA, HFAPS, CWOA, TLABC, NM-MPSO, OBWOA, EHA-NMS, ABC-DE, ABC-TRR, Rcr-IJADE, STLBO, ISCE, and CSO. Moreover, experiments on three different types of commercial PV modules (i.e. mono-crystalline, poly-crystalline, and thin film) at various environmental conditions suggest that the COA is useful and reliable for practical applications. In addition to the excellent fitting accuracy, the COA also produces consistent results. Notably, the STD of the fitness values over 35 runs is observed to be at least five orders of magnitude lower than those published in other studies.

The outstanding performance of COA can primarily be attributed to its unique structure and search mechanisms. For instance, the occasional expulsion of the coyotes from their respective packs promotes population diversity through the exchange of information among the coyote packs. In addition, the utilization of local best solutions, i.e. alphas, dictates the movement of other coyotes during cultural interaction phase results in good exploitation capability. Furthermore, the parametric constraint ensures that the search is always confined within the user-defined boundaries. Meanwhile, the birth and death of the coyotes serves as a mechanism to retain prospective solutions and eliminate weaker ones as the algorithm progresses. Jointly, these features contribute to reliable and consistent solutions. In view of these merits, the proposed COA-based optimizer is envisaged to be a competitive alternative especially in applications where precise extraction of the solar cell parameters is required. It can be useful in applications such as the characterization new PV cells, fault diagnosis of PV systems, as well as the study of solar cell degradation. For future works, the algorithm may be implemented on more specialized PV models of emerging solar cells, e.g. the perovskite, organic and multi-junction.

Declaration of Competing Interest

The authors declare that they have no known competing financial interests or personal relationships that could have appeared to influence the work reported in this paper.

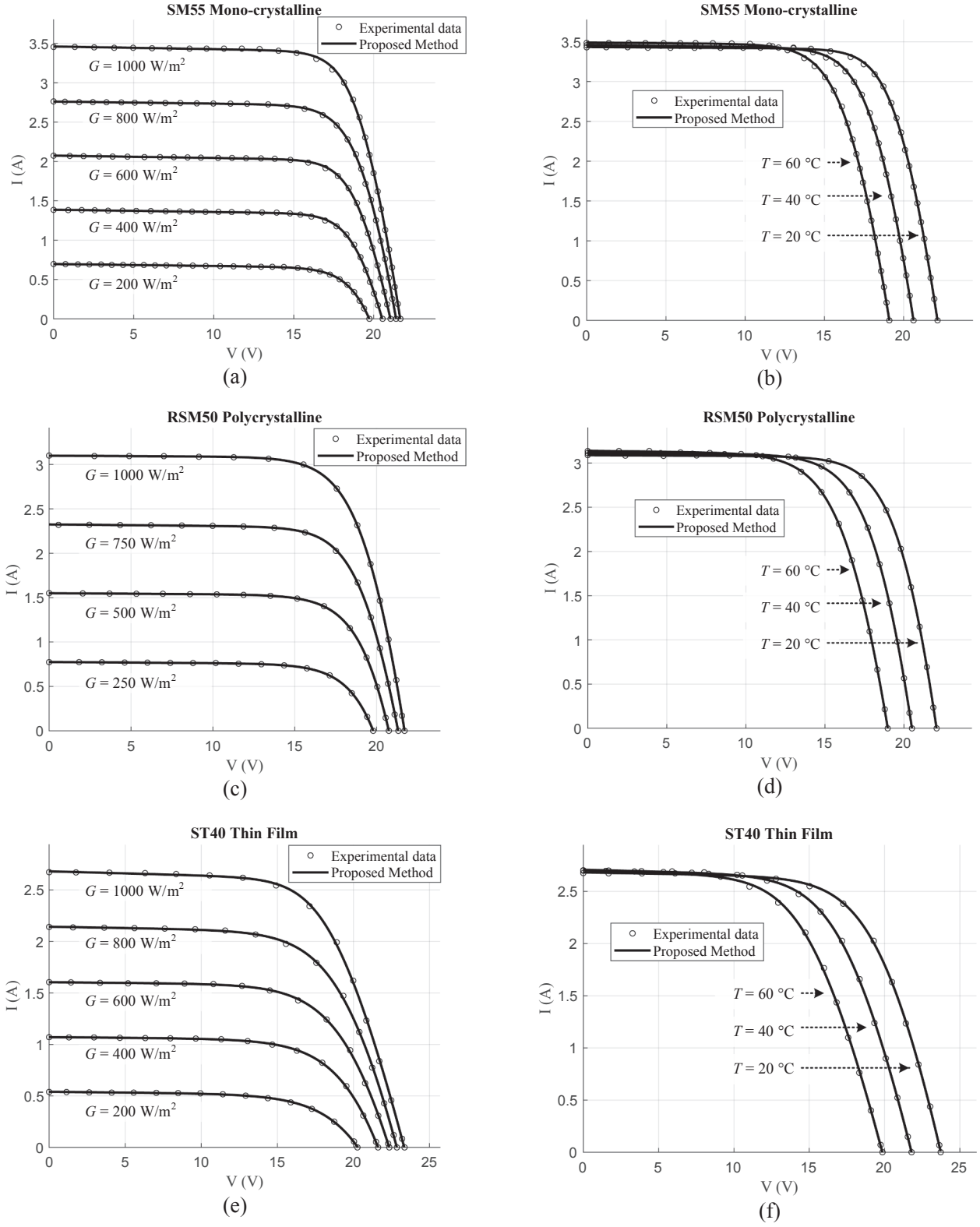

Fig. 10. The computed *I-V* curves and empirical data points for: varying irradiance (a) SM55 mono-crystalline (c) RSM50 poly-crystalline (e) ST40 thin film; and varying temperature (b) SM55 mono-crystalline (d) RSM50 poly-crystalline (f) ST40 thin film.

Acknowledgement

This work was funded by the Ministry of Higher Education, Malaysia, under the Rising Star Grant Award. The grant was managed by the Research Management Centre, Universiti Teknologi Malaysia, Skudai, Malaysia, under Vot. no. R.J130000.7823.4F919.

Appendix A

See Tables A1 and A2.

Table A1
Parameter extraction results for SM55, RSM50, and ST40 PV modules under irradiance variations.

Parameter	SM55 Mono-crystalline	RSM50* Poly-crystalline	ST40 Thin film
$G = 1000\ W/m^2$			
I_{PV}	3.4661	3.0996	2.6952
I_o	7.4921E-10	6.5517E-07	1.3056E-07
a	1.0528	1.5273	1.2868
R_s	0.0132	0.0111	0.0302
R_{sh}	8.2061	30.1255	5.9169
RMSE	0.0135	0.0050	0.0123
$G = 800\ W/m^2$ ($750\ W/m^2$)			
I_{PV}	2.7641	2.3260	2.1488
I_o	8.5671E-09	1.4352E-07	9.2407E-06
a	1.1817	1.3891	1.7176
R_s	0.0126	0.0136	0.0223
R_{sh}	10.6760	16.9692	9.2010
RMSE	0.0097	0.0065	0.0093
$G = 600\ W/m^2$ ($500\ W/m^2$)			
I_{PV}	2.0780	1.5500	1.6060
I_o	2.9004E-10	8.5514E-07	1.6659E-05
a	1.0038	1.5578	1.8076
R_s	0.0174	0.0082	0.0218
R_{sh}	9.1690	24.5878	18.4972
RMSE	0.0061	0.0017	0.0067
$G = 400\ W/m^2$ ($250\ W/m^2$)			
I_{PV}	1.3891	0.7748	1.0722
I_o	3.0616E-10	8.5631E-07	2.5424E-05
a	1.0000	1.5636	1.8857
R_s	0.0201	0.0064	0.0169
R_{sh}	9.7251	22.1517	18.1012
RMSE	0.0078	0.0018	0.0041
$G = 200\ W/m^2$			
I_{PV}	0.6969	–	0.5402
I_o	1.0672E-08	–	4.2246E-05
a	1.1895	–	2.0000
R_s	0.0131	–	0.0143
R_{sh}	11.3179	–	16.6155
RMSE	0.0027	–	0.0032

Table A2
Parameter extraction results for SM55, RSM50, and ST40 PV modules under temperature variations.

Parameter	SM55 Mono-crystalline	RSM50 Poly-crystalline	ST40 Thin film
$T = 20\ ^\circ C$			
I_{PV}	3.4366	3.0891	2.6883
I_o	3.4500E-09	4.7792E-07	6.0178E-06
a	1.1556	1.5212	1.6936
R_s	0.0125	0.0101	0.0218
R_{sh}	20.3143	33.0500	9.3289
RMSE	0.0106	0.0041	0.0089
$T = 40\ ^\circ C$			
I_{PV}	3.4644	3.1139	2.7177
I_o	5.3977E-08	4.3592E-06	1.0701E-05
a	1.2412	1.6450	1.6265
R_s	0.0124	0.0098	0.0254
R_{sh}	11.4250	34.8668	6.7753
RMSE	0.0115	0.0036	0.0097
$T = 60\ ^\circ C$			
I_{PV}	3.4936	3.1415	2.7228
I_o	7.1436E-07	1.4149E-05	1.5580E-05
a	1.3413	1.6681	1.5287
R_s	0.0125	0.0120	0.0288
R_{sh}	16.0267	12.7376	4.8186
RMSE	0.0123	0.0058	0.0144

References

(ISE), F.I.f.S.E.S., 2018. Photovoltaics report.

Abd Elaziz, M., Oliva, D., 2018. Parameter estimation of solar cells diode models by an improved opposition-based whale optimization algorithm. Energy Convers. Manage. 171, 1843–1859.

Alam, D.F., Yousri, D.A., Eteiba, M.B., 2015. Flower Pollination Algorithm based solar PV parameter estimation. Energy Convers. Manage. 101, 410–422.

AlHajri, M.F., El-Naggar, K.M., AlRashidi, M.R., Al-Othman, A.K., 2012. Optimal extraction of solar cell parameters using pattern search. Renewable Energy 44, 238–245.

AlRashidi, M.R., AlHajri, M.F., El-Naggar, K.M., Al-Othman, A.K., 2011. A new estimation approach for determining the I-V characteristics of solar cells. Sol. Energy 85 (7), 1543–1550.

Askarzadeh, A., Rezazadeh, A., 2012. Parameter identification for solar cell models using harmony search-based algorithms. Sol. Energy 86 (11), 3241–3249.

Askarzadeh, A., Rezazadeh, A., 2013a. Artificial bee swarm optimization algorithm for parameters identification of solar cell models. Appl. Energy 102, 943–949.

Askarzadeh, A., Rezazadeh, A., 2013b. Extraction of maximum power point in solar cells using bird mating optimizer-based parameters identification approach. Sol. Energy 90, 123–133.

Beigi, A.M., Maroosi, A., 2018. Parameter identification for solar cells and module using a hybrid firefly and pattern search algorithms. Sol. Energy 171, 435–446.

Bekoff, M., 1977. Canis latrans. Mammalian species 79, 1–9.

Ben Or, A., Appelbaum, J., 2013. Estimation of multi-junction solar cell parameters. Prog. Photovoltaics Res. Appl. 21 (4), 713–723.

Chan, D.S.H., Phang, J.C.H., 1987. Analytical methods for the extraction of solar-cell single- and double-diode model parameters from I-V characteristics. Elect. Dev. IEEE Trans. 34 (2), 286–293.

Chegaar, M., Ouennoughi, Z., Hoffmann, A., 2001. A new method for evaluating illuminated solar cell parameters. Solid-State Electron. 45 (2), 293–296.

Chen, X., Xu, B., Mei, C., Ding, Y., Li, K., 2018. Teaching–learning–based artificial bee colony for solar photovoltaic parameter estimation. Appl. Energy 212, 1578–1588.

Chen, X., Yu, K., Du, W., Zhao, W., Liu, G., 2016a. Parameters identification of solar cell models using generalized oppositional teaching learning based optimization. Energy 99, 170–180.

Chen, Z., Wu, L., Lin, P., Wu, Y., Cheng, S., 2016b. Parameters identification of photovoltaic models using hybrid adaptive nelder-mead simplex algorithm based on eagle strategy. Appl. Energy 182, 47–57.

Chin, V.J., Salam, Z., 2018. Modifications to Accelerate the Iterative Algorithm for the Two-diode Model of PV Module. In: 2018 IEEE PES Asia-Pacific Power and Energy Engineering Conference (APPEEC). IEEE, pp. 200–205.

Chin, V.J., Salam, Z., 2019. A new three-point-based approach for the parameter extraction of photovoltaic cells. Appl. Energy 237, 519–533.

Chin, V.J., Salam, Z., Ishaque, K., 2015a. An accurate two diode model computation for CIS thin film PV module using the hybrid approach, Electric Power and Energy Conversion Systems (EPECS). In: 2015 4th International Conference on. pp. 1-6.

Chin, V.J., Salam, Z., Ishaque, K., 2015b. Cell modelling and model parameters estimation techniques for photovoltaic simulator application: a review. Appl. Energy 154, 500–519.

Chin, V.J., Salam, Z., Ishaque, K., 2015c. An improved method to estimate the parameters of the single diode model of photovoltaic module using differential evolution, Electric Power and Energy Conversion Systems (EPECS). In: 2015 4th International Conference on. pp. 1-6.

Chin, V.J., Salam, Z., Ishaque, K., 2016. An accurate modelling of the two-diode model of PV module using a hybrid solution based on differential evolution. Energy Convers. Manage. 124, 42–50.

Chin, V.J., Salam, Z., Ishaque, K., 2017. An accurate and fast computational algorithm for the two-diode model of PV module based on hybrid method. IEEE Trans. Ind. Electron. 64 (8), 6212–6222.

Coelho, J.P.L.d.S., 2018. Coyote Optimization Algorithm: A new metaheuristic for global optimization. In: IEEE Congress on Evolutionary Computation (CEC). Rio de Janeiro, Brazil, pp. 2633–2640.

Conner, M.M., Ebinger, M.R., Knowlton, F.F., 2008. Evaluating coyote management strategies using a spatially explicit, individual-based, socially structured population model. Ecol. Model. 219 (1–2), 234–247.

da Costa, W.T., Fardin, J.F., Simonetti, D.S.L., Neto, L.d.V.B.M., 2010. Identification of photovoltaic model parameters by Differential Evolution, Industrial Technology (ICIT). In: 2010 IEEE International Conference on. pp. 931–936.

Davis, M.W., Fanney, A.H., Dougherty, B.P., 2001. Prediction of building integrated photovoltaic cell temperatures. J. Sol. Energy Eng. 123 (3), 200–210.

De Castro, F., Laudani, A., Fulginei, F.R., Salvini, A., 2016. An in-depth analysis of the modelling of organic solar cells using multiple-diode circuits. Sol. Energy 135, 590–597.

Dkhichi, F., Oukarfi, B., Fakkar, A., Belbounaguia, N., 2014. Parameter identification of solar cell model using levenberg–marquardt algorithm combined with simulated annealing. Sol. Energy 110, 781–788.

Easwarakhanthan, T., Bottin, J., Bouhouch, I., Boutrit, C., 1986. Nonlinear minimization algorithm for determining the solar cell parameters with microcomputers. Int. J. Solar Energy 4 (1), 1–12.

Eiben, A.E., Hinterding, R., Michalewicz, Z., 1999. Parameter control in evolutionary algorithms. IEEE Trans. Evol. Comput. 3 (2), 124–141.

El-Naggar, K.M., AlRashidi, M.R., AlHajri, M.F., Al-Othman, A.K., 2012. Simulated Annealing algorithm for photovoltaic parameters identification. Sol. Energy 86 (1), 266–274.

Elbaset, A.A., Ali, H., Abd-El Sattar, M., 2014. Novel seven-parameter model for photovoltaic modules. Sol. Energy Mater. Sol. Cells 130, 442–455.

Femia, N., Petrone, G., Spagnuolo, G., Vitelli, M., 2012. Power Electronics and Control Techniques for Maximum Energy Harvesting in Photovoltaic Systems. CRC Press.

Gao, X., Cui, Y., Hu, J., Xu, G., Wang, Z., Qu, J., Wang, H., 2018. Parameter extraction of solar cell models using improved shuffled complex evolution algorithm. Energy Convers. Manage. 157, 460–479.

Gong, W., Cai, Zhihua, 2013. Parameter extraction of solar cell models using repaired adaptive differential evolution. Sol. Energy 94.

Gow, J.A., Manning, C.D., 1999. Development of a photovoltaic array model for use in power-electronics simulation studies. Elect. Pow. Appl. IEE Proc. 146 (2), 193–200.

Guo, L., Meng, Z., Sun, Y., Wang, L., 2016. Parameter identification and sensitivity analysis of solar cell models with cat swarm optimization algorithm. Energy Convers. Manage. 108, 520–528.

Hachana, O., Hemsas, K.E., Tina, G.M., Ventura, C., 2013. Comparison of different metaheuristic algorithms for parameter identification of photovoltaic cell/module. J. Renew. Sust. Energy 5 (5).

Hamid, N.F.A., Rahim, N.A., Selvaraj, J., 2016. Solar cell parameters identification using hybrid Nelder-Mead and modified particle swarm optimization. J. Renewable Sustainable Energy 8 (1), 015502.

Han, W., Wang, H.-H., Chen, L., 2014. Parameters identification for photovoltaic module based on an improved artificial fish swarm algorithm. Sci. World J. 2014, 859239.

Hasan, M.A., Parida, S.K., 2016. An overview of solar photovoltaic panel modeling based on analytical and experimental viewpoint. Renew. Sustain. Energy Rev. 60, 75–83.

Hengsi, Q., Kimball, J.W., 2011. Parameter determination of Photovoltaic Cells from field testing data using particle swarm optimization. In: Power and Energy Conference at Illinois (PECI), 2011 IEEE. pp. 1-4.

Ikegami, T., Maezono, T., Nakanishi, F., Yamagata, Y., Ebihara, K., 2001. Estimation of equivalent circuit parameters of PV module and its application to optimal operation of PV system. Sol. Energy Mater. Sol. Cells 67 (1), 389–395.

Ishaque, K., Salam, Z., Mekhilef, S., Shamsudin, A., 2012. Parameter extraction of solar photovoltaic modules using penalty-based differential evolution. Appl. Energy 99, 297–308.

Ishaque, K., Salam, Z., Taheri, H., Shamsudin, A., 2011. A critical evaluation of EA computational methods for photovoltaic cell parameter extraction based on two diode model. Sol. Energy 85 (9), 1768–1779.

Jain, A., Kapoor, A., 2005. A new approach to study organic solar cell using lambert W-function. Sol. Energy Mater. Sol. Cells 86 (2), 197–205.

Jamadi, M., Merrikh-Bayat, F., Bigdeli, M., 2016. Very accurate parameter estimation of single- and double-diode solar cell models using a modified artificial bee colony algorithm. Int. J. Energy Environ. Eng. 7 (1), 13–25.

Jamil, W.J., Rahman, H.A., Shaari, S., Salam, Z., 2017. Performance degradation of photovoltaic power system: Review on mitigation methods. Renew. Sustain. Energy Rev. 67, 876–891.

Jervase, J.A., Bourdoucen, H., Al-Lawati, A., 2001. Solar cell parameter extraction using genetic algorithms. Meas. Sci. Technol. 12 (11), 1922.

Jiang, L.L., Maskell, D.L., Patra, J.C., 2013. Parameter estimation of solar cells and modules using an improved adaptive differential evolution algorithm. Appl. Energy 112, 185–193.

Jing Jun, S., Kay-Soon, L., 2012. Photovoltaic model identification using particle swarm optimization with inverse barrier constraint. Pow. Elect. IEEE Trans. 27 (9), 3975–3983.

Kahoul, N., Houabes, M., Sadok, M., 2014. Assessing the early degradation of photovoltaic modules performance in the Saharan region. Energy Convers. Manage. 82, 320–326.

Kichou, S., Silvestre, S., Nofuentes, G., Torres-Ramírez, M., Chouder, A., Guasch, D., 2016. Characterization of degradation and evaluation of model parameters of amorphous silicon photovoltaic modules under outdoor long term exposure. Energy 96, 231–241.

Kler, D., Sharma, P., Banerjee, A., Rana, K.P.S., Kumar, V., 2017. PV cell and module efficient parameters estimation using evaporation rate based water cycle algorithm. Swarm Evol. Comput. 35 (Supplement C), 93–110.

Kurtz, S., Whitfield, K., TamizhMani, G., Koehl, M., Miller, D., Joyce, J., Wohlgemuth, J., Bosco, N., Kempe, M., Zgonena, T., 2011. Evaluation of high-temperature exposure of photovoltaic modules. Prog. Photovoltaics Res. Appl. 19 (8), 954–965.

Lin, P., Cheng, S., Yeh, W., Chen, Z., Wu, L., 2017. Parameters extraction of solar cell models using a modified simplified swarm optimization algorithm. Solar Energy 144 (Supplement C), 594–603.

Lorenz, E., Hurka, J., Heinemann, D., Beyer, H.G., 2009. Irradiance forecasting for the power prediction of grid-connected photovoltaic systems. Selected topics in applied earth observations and remote sensing. IEEE J. 2 (1), 2–10.

Ma, J., Ting, T.O., Man, K.L., Zhang, N., Guan, S.-U., Wong, P.W.H., 2013. Parameter estimation of photovoltaic models via cuckoo search. J. Appl. Math. 2013, 8.

Mäki, A., Valkealahti, S., 2012. Power losses in long string and parallel-connected short strings of series-connected silicon-based photovoltaic modules due to partial shading conditions. IEEE Trans. Energy Convers. 27 (1), 173–183.

Malvoni, M., De Giorgi, M.G., Congedo, P.M., 2017. Study of degradation of a grid connected photovoltaic system. Energy Procedia 126, 644–650.

Mellit, A., Pavan, A.M., 2010. A 24-h forecast of solar irradiance using artificial neural network: Application for performance prediction of a grid-connected PV plant at Trieste. Italy. Solar Energy 84 (5), 807–821.

Meyer, E.L., Dyk, E.E.V., 2004. Assessing the reliability and degradation of photovoltaic module performance parameters. IEEE Trans. Reliab. 53 (1), 83–92.

Moeini, I., Ahmadpour, M., Mosavi, A., Alharbi, N., Gorji, N.E., 2018. Modeling the time-dependent characteristics of perovskite solar cells. Sol. Energy 170, 969–973.

Moldovan, N., Picos, R., Garcia-Moreno, E., 2009. Parameter Extraction of a Solar Cell

Compact Model usign Genetic Algorithms, Electron Devices, 2009. In: CDE 2009. Spanish Conference on. pp. 379-382.
Oliva, D., Abd El Aziz, M., Ella Hassanien, A., 2017a. Parameter estimation of photovoltaic cells using an improved chaotic whale optimization algorithm. Appl. Energy 200, 141–154.
Oliva, D., Cuevas, E., Pajares, G., 2014. Parameter identification of solar cells using artificial bee colony optimization. Energy 72, 93–102.
Oliva, D., Ewees, A.A., Aziz, M.A.E., Hassanien, A.E., Peréz-Cisneros, M., 2017b. A Chaotic improved artificial bee colony for parameter estimation of photovoltaic cells. Energies 10 (7), 865.
Park, N., Oh, W., Kim, D., 2013. Effect of temperature and humidity on the degradation rate of multicrystalline silicon photovoltaic module. Int. J. Photoenergy 2013.
Pitt, W.C., Box, P.W., Knowlton, F.F., 2003. An individual-based model of canid populations: modelling territoriality and social structure. Ecol. Model. 166 (1–2), 109–121.
Poulek, V., Matuška, T., Libra, M., Kachalouski, E., Sedláček, J., 2018. Influence of increased temperature on energy production of roof integrated PV panels. Energy Build. 166, 418–425.
Pourmousa, N., Ebrahimi, S.M., Malekzadeh, M., Alizadeh, M., 2019. Parameter estimation of photovoltaic cells using improved Lozi map based chaotic optimization algorithm. Sol. Energy 180, 180–191.
Rajput, P., Shyam, Tomar, V., Tiwari, G.N., Sastry, O.S., Bhatti, T.S., 2018. A thermal model for N series connected glass/cell/polymer sheet and glass/cell/glass crystalline silicon photovoltaic modules with hot solar cells connected in series and its thermal losses in real outdoor condition. Renewable Energy 126, 370–386.
Rajput, P., Tiwari, G.N., Sastry, O.S., 2016a. Thermal modelling and experimental validation of hot spot in crystalline silicon photovoltaic modules for real outdoor condition. Sol. Energy 139, 569–580.
Rajput, P., Tiwari, G.N., Sastry, O.S., Bora, B., Sharma, V., 2016b. Degradation of monocrystalline photovoltaic modules after 22years of outdoor exposure in the composite climate of India. Sol. Energy 135, 786–795.
Ram, J.P., Manghani, H., Pillai, D.S., Babu, T.S., Miyatake, M., Rajasekar, N., 2018. Analysis on solar PV emulators: A review. Renew. Sustain. Energy Rev. 81, 149–160.
Saha, P., Kumar, S., Nayak, S.K., Sahu, H.S., 2015. Parameter estimation of double diode photo-voltaic module, Power, Dielectric and Energy Management at NERIST (ICPDEN). In: 2015 1st Conference on. IEEE, pp. 1-4.
Sandrolini, L., Artioli, M., Reggiani, U., 2010. Numerical method for the extraction of photovoltaic module double-diode model parameters through cluster analysis. Appl. Energy 87 (2), 442–451.
Secretariat, R., 2018. Renewables 2018 global status report, renewables global status report (GSR).
Sellami, A., Bouaïcha, M., 2011. Application of the genetic algorithms for identifying the electrical parameters of PV solar generators. In: Leonid A. Kosyachenko, (Ed.). Solar Cells-Silicon Wafer-Based Technologies. ISBN, 978-953.
Strevel, N., Trippel, L., Gloeckler, M., 2012. Performance characterization and superior energy yield of First Solar PV power plants in high-temperature conditions. Photovoltaics International 17 (3), 148–154.
Tan, K.C., Chiam, S.C., Mamun, A.A., Goh, C.K., 2009. Balancing exploration and exploitation with adaptive variation for evolutionary multi-objective optimization. Eur. J. Oper. Res. 197 (2), 701–713.
Villalva, M.G., Gazoli, J.R., Filho, E.R., 2009. Comprehensive approach to modeling and simulation of photovoltaic arrays. IEEE Trans. Pow. Elect. 24 (5), 1198–1208.
Virtuani, A., Strepparava, D., 2017. Modelling the performance of amorphous and crystalline silicon in different typologies of building-integrated photovoltaic (BIPV) conditions. Sol. Energy 146, 113–118.
Wei, H., Cong, J., Lingyun, X., Deyun, S., 2011. Extracting solar cell model parameters based on chaos particle swarm algorithm, Electric Information and Control Engineering (ICEICE). In: 2011 International Conference on. IEEE, pp. 398–402.
Wolpert, D.H., Macready, W.G., 1997. No free lunch theorems for optimization. IEEE Trans. Evol. Comput. 1 (1), 67–82.
Wu, L., Chen, Z., Long, C., Cheng, S., Lin, P., Chen, Y., Chen, H., 2018. Parameter extraction of photovoltaic models from measured I-V characteristics curves using a hybrid trust-region reflective algorithm. Appl. Energy 232, 36–53.
Xiong, G., Zhang, J., Yuan, X., Shi, D., He, Y., Yao, G., 2018. Parameter extraction of solar photovoltaic models by means of a hybrid differential evolution with whale optimization algorithm. Sol. Energy 176, 742–761.
Xu, S., Wang, Y., 2017. Parameter estimation of photovoltaic modules using a hybrid flower pollination algorithm. Energy Convers. Manage. 144, 53–68.
Yang, D., Dong, Z., Reindl, T., Jirutitijaroen, P., Walsh, W.M., 2014. Solar irradiance forecasting using spatio-temporal empirical kriging and vector autoregressive models with parameter shrinkage. Sol. Energy 103, 550–562.
Ye, M., Wang, X., Xu, Y., 2009. Parameter extraction of solar cells using particle swarm optimization. J. Appl. Phys. 105 (9), 094502.
Yu, F., Huang, G., Lin, W., Xu, C., 2018a. Lumped-Parameter Equivalent Circuit Model for S-Shaped Current-Voltage Characteristics of Organic Solar Cells. IEEE Trans. Elect. Dev. 1–8.
Yu, K., Chen, X., Wang, X., Wang, Z., 2017. Parameters identification of photovoltaic models using self-adaptive teaching-learning-based optimization. Energy Convers. Manage. 145, 233–246.
Yu, K., Liang, J.J., Qu, B.Y., Cheng, Z., Wang, H., 2018b. Multiple learning backtracking search algorithm for estimating parameters of photovoltaic models. Appl. Energy 226, 408–422.
Yuan, X., Xiang, Y., He, Y., 2014. Parameter extraction of solar cell models using mutative-scale parallel chaos optimization algorithm. Sol. Energy 108, 238–251.
Zagrouba, M., Sellami, A., Bouaïcha, M., Ksouri, M., 2010. Identification of PV solar cells and modules parameters using the genetic algorithms: Application to maximum power extraction. Sol. Energy 84 (5), 860–866.
Zhang, Y., Lin, P., Chen, Z., Cheng, S., 2016. A population classification evolution algorithm for the parameter extraction of solar cell models. Int. J. Photoenergy 2016.